The Astrophysical Journal, 677:1296–1308, 2008 April 20

NUMERICAL SIMULATION OF DUST AGGREGATE COLLISIONS. II. COMPRESSION AND DISRUPTION OF THREE-DIMENSIONAL AGGREGATES IN HEAD-ON COLLISIONS

Koji Wada, Hidekazu Tanaka, Toru Suyama, Hiroshi Kimura, and Tetsuo Yamamoto
Institute of Low Temperature Science, Hokkaido University, Sapporo 060-0819, Japan; wada@neko.lowtem.hokudai.ac.jp
Received 2007 September 20; accepted 2008 January 14

ABSTRACT

We study collisions between dust aggregates to construct a model of their structural evolution in protoplanetary disks. We carry out three-dimensional simulations of aggregate collisions and examine their compression and disruption processes following our previous two-dimensional simulations. We take clusters of ballistic cluster-cluster aggregation (BCCA) formed by a hit-and-stick process as initial structures and study their head-on collisions with the use of realistic binding forces. Our numerical results indicate that the energy criteria for compression and disruption of BCCA clusters are consistent with previous two-dimensional simulations. For aggregate compression at a collision, we succeed in obtaining a scaling law in which the gyration radius of the resultant aggregate is proportional to $E_{\rm imp}^{-0.10}$, where $E_{\rm imp}$ is the impact energy. Furthermore, we derive an "equation of state" of aggregates which reproduces the scaling law for compression. The equation of state is useful for describing the density evolution of dust aggregates during their growth.

Subject headings: circumstellar matter — dust, extinction — methods: *n*-body simulations — planetary systems: formation — planetary systems: protoplanetary disks

1. INTRODUCTION

The structural evolution of dust aggregates is a key for understanding planetesimal formation processes in protoplanetary disks. Planetesimals form through collisions between dust aggregates composed of a large number of submicron particles and/or gravitational instability of the dust layer in the midplane of the disks (e.g., Goldreich & Ward 1973; Weidenschilling & Cuzzi 1993). Dust aggregates cannot prevent themselves from growing by mutual collisions in the early growth stages of planetary system formation. In such growth processes, coupling of dust with disk gas plays an important role in the orbital motion of dust aggregates (e.g., Adachi et al. 1976; Weidenschilling 1980, 1984; Nakagawa et al. 1981; Tanaka et al. 2005). The degree of coupling with disk gas is determined by the surface-to-mass ratios of dust aggregates, which depend on their collisional history. Therefore, it is important to reveal the evolution of aggregate structures during collisional growth.

A high degree of coupling leads to a significantly low impact velocity (<1 mm s^{-1}) between aggregates and makes their structure very fluffy. Actually, in such a low-velocity collision, aggregates would just stick without any compression, resulting in clusters of ballistic cluster-cluster aggregation (BCCA) with a fractal dimension between $\sim$1.5 and $\sim$2 (Meakin 1991; Mukai et al. 1992; Krause & Blum 2004; Paszun & Dominik 2006). When such BCCA clusters grow and their impact energies become large enough, they begin to be compressed. Once aggregates are compressed, the surface-to-mass ratios are reduced and then the impact velocities increase, resulting in further compaction of the aggregates. In extremely high velocity collisions, aggregates would be disrupted. Hence, it is necessary to clarify when and how aggregates are compressed or disrupted during their collisions.

Several studies on dust growth took into account the structural evolution (e.g., Ossenkopf 1993; Weidenschilling & Ruzmaikina 1994; Kempf et al. 1999; Blum 2004; Ormel et al. 2007). However, dust structures in their models are too oversimplified to construct a realistic model of dust growth. A further study of the structural evolution requires a thorough examination of compression and disruption of dust aggregates. Sirono (2004) and Schäfer et al. (2007) performed numerical simulations of dust collisions by means of a smoothed particle hydrodynamic code. They showed that the compressive strength of dust should be less than its tensile strength for sticking and growing of dust. Their dust is expressed by a continuum medium, which requires a fracture model and an equation of state (EOS) to simulate compression and disruption of aggregates. They used an EOS of aggregates of toner particles applicable to the density range $\gtrsim$0.1 g cm^{-3} for relatively compact aggregates. On the other hand, the density of BCCA clusters we consider is lower than this density range by several orders of magnitude. One needs an EOS applicable to such low-density aggregates.

Dominik & Tielens (1997) carried out two-dimensional (2D) numerical simulations of aggregate collisions.[1] They modeled particle interactions in detail and calculated the motion of each particle directly in their simulation. Table 1 summarizes the dependence of collisional outcomes on the impact energy $E_{\rm imp}$ they obtained, which we call the "DT recipe." The recipe is expressed in terms of three parameters, $E_{\rm roll}$, $E_{\rm break}$, and n_k. The energy necessary to roll a particle by 90° on the other particle in contact is denoted by $E_{\rm roll}$ and is given by

$$E_{\rm roll} = 12\pi^2\gamma R\xi_{\rm crit}, \tag{1}$$

where γ is the surface energy, $R = (1/r_1 + 1/r_2)^{-1}$ is the reduced radius of the particles of radii r_1 and r_2, and $\xi_{\rm crit}$ is the critical rolling displacement (Dominik & Tielens 1995, 1997; Wada et al. 2007). The energy necessary to break one contact, $E_{\rm break}$, is given by

$$E_{\rm break} \simeq 1.54F_c\delta_c, \tag{2}$$

where $F_c = 3\pi\gamma R$ is the force needed to separate two particles in contact and δ_c is the critical compression length between the

[1] Exactly speaking, their simulations were not purely 2D; they did not simulate motion of disks but spheres moving in a plane.

TABLE 1
RECIPE FOR THE OUTCOMES OF AGGREGATE COLLISIONS PROPOSED BY DOMINIK & TIELENS (1997)

Energy	Collisional Outcome
$E_{\rm imp} \simeq 5E_{\rm roll}$	First visible restructuring
$E_{\rm imp} \simeq n_k E_{\rm roll}$	Maximum compression
$E_{\rm imp} \simeq 3n_k E_{\rm break}$	Loss of one particle
$E_{\rm imp} \gtrsim 10n_k E_{\rm break}$	Catastrophic disruption

particles in contact (Chokshi et al. 1993; Wada et al. 2007). We define n_k as the number of contacts in aggregates before impact. The numerical simulation of Dominik & Tielens (1997) is limited to 2D and head-on collisions of one type of BCCA-like initial structure containing as few as 40 particles. Developing a new numerical code, we extended their numerical simulations of 2D aggregate collisions by using various initial structures of BCCA clusters composed of a large number (up to 2048) of particles (Wada et al. 2007). We confirmed the criteria by Dominik & Tielens (1997) for maximum compression and catastrophic disruption of the collisional aggregates. In addition, we found empirical scaling laws for the gyration radius and the number of contacts of resultant aggregates formed after collisions. Although the DT recipe seems to explain the experimental results of small aggregate ($\sim$60 particles) collisions by Blum & Wurm (2000), it is insufficient to model the structural evolution of dust aggregates in protoplanetary disks.

In this paper, we carry out three-dimensional (3D) simulations of aggregate collisions, using the numerical code developed in Wada et al. (2007). The results from 3D simulations will provide us with a more realistic model for the structural evolution of dust aggregates. The scaling laws and the "EOS" of aggregates obtained from an analysis of the numerical results will be applicable to the study of the growth of dust to planetesimals. Sirono & Greenberg (2000) formulated an EOS of aggregates analytically, assuming that the aggregates consist of periodically arranged chains of particles. For more realistic aggregates, the numerically derived EOS will be useful. It is of course difficult to directly simulate collisions of large aggregates, say, of a cm size, consisting of more than billions of submicron particles. Therefore, we will reveal the dependence of collisional outcomes on the number of particles composing aggregates and then extrapolate the results to larger sizes.

We here focus on the simplest case, namely, head-on collisions of nonrotating 3D BCCA clusters as the first step of our study on 3D aggregate collisions. Head-on collisions will create the most compressed aggregates. The influence of rotation (Paszun & Dominik 2006) and offset collisions (Sirono 2004; Schäfer et al. 2007; Wada et al. 2007) on collisions of aggregates will be studied in a future work.

In the next section, we briefly describe our numerical code, the parameters used in our simulation, and the initial structures of aggregates. We show our results of 3D simulation for aggregates composed of up to 16,384 particles in § 3. We focus on compression and disruption of the aggregates. We will derive scaling laws for the gyration radius and the number of contacts of the resultant aggregates from our numerical results. In § 4 we derive an EOS of aggregates from the scaling law for compression. Here, the EOS means a relation between the pressure (or the strength) of aggregates and their bulk density. We compare the EOS with that derived analytically by Sirono & Greenberg (2000). Our EOS is applicable to a macroscopic description of aggregate compression. Our macroscopic description will be further tested by Suyama et al. (2008), who directly calculate the growth of aggregates by successive collisions using the same numerical code as that used in the present paper. A summary is given in § 5.

2. NUMERICAL MODEL AND PARAMETERS

We perform 3D simulations of aggregate collisions by the use of the particle interaction model and the numerical code developed by Wada et al. (2007). Here, we briefly describe our numerical code, the parameters used in our simulation, and the initial structures of aggregates.

We directly calculate the motion of each particle, taking into account all mechanical interactions between particles in contact. The contact theory of adhesive elastic spheres determines the interactions for each degree of motion (normal motion, sliding, rolling, and twisting). Normal to the contact plane of two particles, a repulsive or an attractive force acts on them depending on the distance between the centers of the two particles (Johnson et al. 1971; Johnson 1987). Forces and torques against sliding, rolling, and twisting are also exerted on the contact particles (Dominik & Tielens 1995, 1996).

To describe the forces and the torques, Wada et al. (2007) introduced a potential energy, which assures the energy conservation in the elastic regime with high accuracy in the numerical simulations. The potential U consists of the potentials for each degree of motion such that

$$U = U_n(\delta) + U_s(\boldsymbol{\zeta}) + U_r(\boldsymbol{\xi}) + U_t(\boldsymbol{\phi}), \tag{3}$$

where U_n, U_s, U_r, and U_t are the potential energies for the motions of normal direction, sliding, rolling, and twisting, respectively. These potentials are functions of each displacement (the normal compression distance δ, the sliding displacement $\boldsymbol{\zeta}$, the rolling displacement $\boldsymbol{\xi}$, and the twisting angle $\boldsymbol{\phi}$; see Fig. 2 of Wada et al. 2007). Differentiation of U by each displacement yields the forces and the torques exerted on the particles in contact (see Wada et al. 2007 for detail).

Energy dissipation occurs at the moments of contact and separation of particles because of excitation of elastic waves (Chokshi et al. 1993). In our model, the amount of energy dissipated in these moments is given by $0.847F_c\delta_c$ for the contact and $0.089F_c\delta_c$ for the separation (Wada et al. 2007). When the displacements due to sliding, rolling, and twisting exceed the elastic limits, the mechanical energy is also dissipated. The amount of energy dissipation is proportional to the critical displacements (see eq. [1]). The most important critical displacement is the critical rolling displacement $\xi_{\rm crit}$ in low-velocity collisions, because aggregates are compressed through rolling motion, on which most energy is dissipated. However, $\xi_{\rm crit}$ has a large uncertainty ranging from 2 to 32 Å (Dominik & Tielens 1995; Heim et al. 1999). In our simulation, therefore, we put $\xi_{\rm crit}$ as a parameter and set $\xi_{\rm crit} = 2$, 8, or 30 Å.

We consider aggregates composed of a large number of spherical particles with radius of $r_1 = 0.1$ μm made of quartz or ice. Material parameters used in the calculation are shown in Table 2. As initial aggregates before collisions, we prepare 3D BCCA clusters produced by successive "head-on" sticking of two identical aggregates in the following procedure: (1) prepare an aggregate composed of i particles (initially $i = 2$), (2) copy this aggregate and make the copy oriented in a randomly chosen direction, (3) by head-on sticking of these two, make a new aggregate composed of $2i$ particles, (4) continue the procedure (1)–(3) until an aggregate composed of N_0 particles is produced. The number of particles composing the initial clusters is set to $N_0 = 512$, 2048, or 8192 (see Fig. 1). The relation between the number of particles N_0

TABLE 2
MATERIAL PARAMETERS

Material	γ (mJ m^{-2})	E (GPa)	ν	ρ_m (kg m^{-3})
Ice.....	100	7	0.25	1000
Quartz.....	25	54	0.17	2600

NOTES.—We have that γ is the surface energy, E is Young's modulus, ν is Poisson's ratio, and ρ_m is material density. All the data except for the γ of ice are the same as used in Dominik & Tielens (1997). The datum of γ of ice is taken from Israelachvili (1992).

and the gyration radius $r_{g,\mathrm{BCCA}}$ of the BCCA clusters produced by such a procedure is expressed as

$$N_0 \sim \left(\frac{r_{g,\mathrm{BCCA}}}{r_1}\right)^{d_f}, \tag{4}$$

where d_f is the fractal dimension of the clusters (e.g., Mukai et al. 1992). We find that d_f for BCCA clusters made by "head-on" collisions is 1.99 as shown in Figure 2. Strictly speaking, such clusters are different from common hit-and-stick BCCA clusters produced by random offset sticking of two clusters of the same mass and different structures (e.g., Smirnov 1990). However, the fractal dimension of the BCCA clusters we produced is close to that of the common BCCA clusters. For a statistical study of numerical results, we choose 10 types of initial BCCA clusters produced by the procedure stated above.

The number of contacts in a BCCA cluster is given by $n_k = N_0 - 1$. The aggregates consisting of 512 particles are used to investigate the dependence of collisional outcomes on the materials and the critical rolling displacement ξ_{crit}. We also use the aggregates of 2048 and 8192 particles in the case of ice and $\xi_{\mathrm{crit}} = 8$ Å to see the dependence on the number of particles.

We perform simulations of head-on collisions of two identical BCCA clusters in the center-of-mass system. The impact energy E_{imp} is given by $E_{\mathrm{imp}} = (1/2)N_{\mathrm{total}}m_1(u_{\mathrm{imp}}/2)^2$, where N_{total} is the sum of the number of particles of two colliding aggregates, m_1 is the mass of one particle, and u_{imp} is the relative impact velocity. We change u_{imp} from 0.024 to 57 m s^{-1} for collisions of ice aggregates and from 0.0096 to 5.7 m s^{-1} for quartz to cover the whole region ranging from no restructuring to catastrophic disruption.

3. RESULTS

In our analysis of collisional outcomes (see Fig. 3 for example), we examine the gyration radius, the number of contacts, and the number of particles of the merged aggregates to see the compression process and the degree of disruption. We take the average of 10 numerical results for initial aggregates having different structures produced by sticking aggregates with random orientations (see § 2).

3.1. *Gyration Radius*

The gyration radius r_g of an aggregate is defined by

$$r_g = \sqrt{\frac{1}{N}\sum_i |\boldsymbol{x}_i - \boldsymbol{x}_M|^2}, \tag{5}$$

where $\boldsymbol{x}_i$ is the position vector of particle i, $\boldsymbol{x}_M$ is that of the center of mass of the aggregate, and N is the number of particles in the aggregate. The gyration radius is a measure of the aggregate size, which changes by restructuring or compression (see Fig. 3).

Figure 4 shows the gyration radius of aggregates after a collision as a function of the impact energy E_{imp}. The gyration radius r_g is normalized by $r_1 N_{\mathrm{large}}^{1/3}$, where N_{large} is the number of particles in the largest aggregate formed by a collision. If the aggregate is disrupted, r_g is calculated for the largest fragment. For

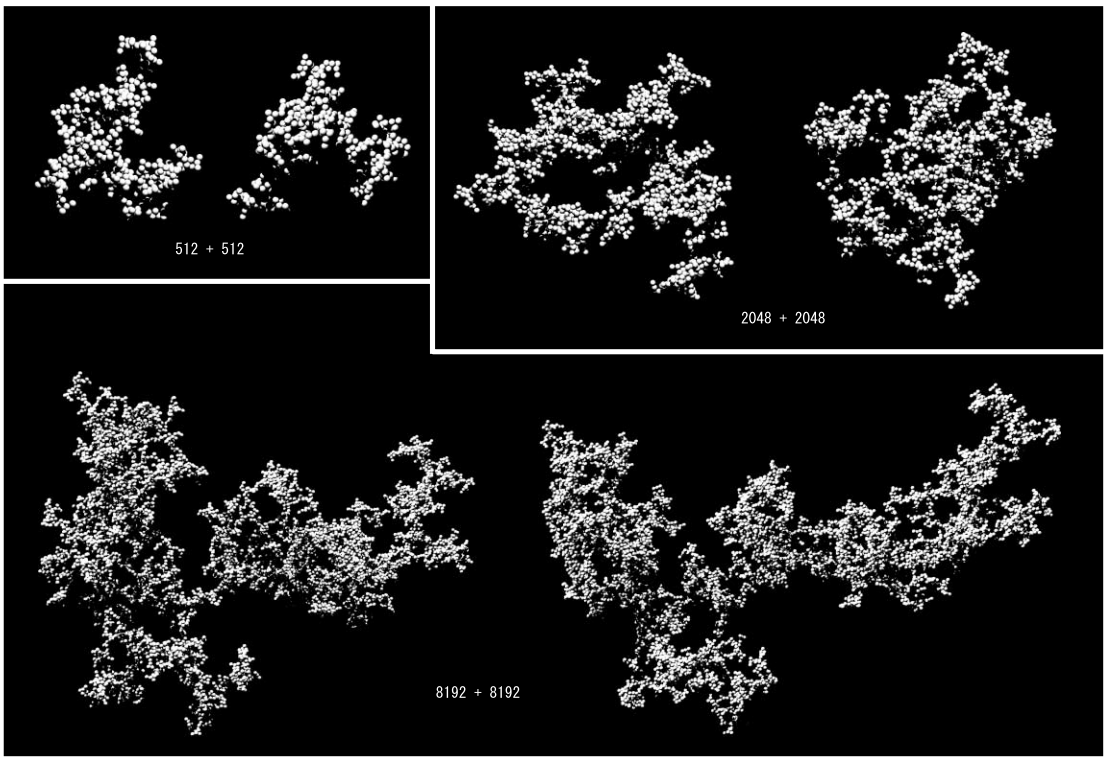

FIG. 1.—Examples of initial BCCA clusters. These aggregates collide with each other horizontally. Each aggregate consists of 512, 2048, or 8192 identical particles.

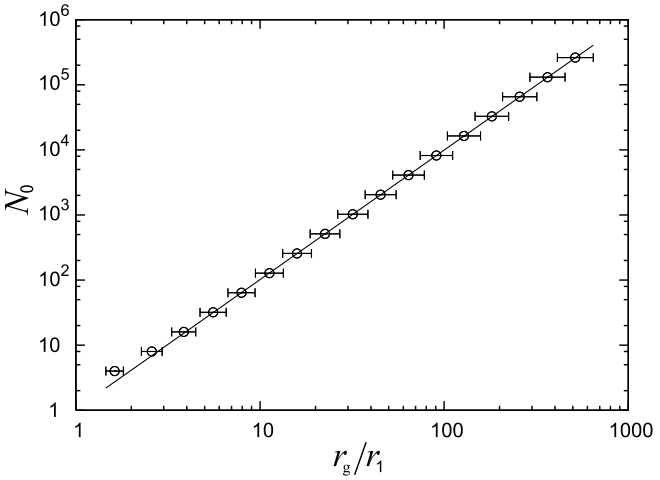

FIG. 2.—Number of particles N_0 in 3D BCCA clusters against their gyration radius r_g normalized by the particle radius r_1. The circles represent the averaged data with error bars of 1 σ, obtained by using 10,000 BCCA clusters produced by head-on sticking. A fitting line (for $N_0 \geq 32$) indicated by the solid line is given by $N_0 = 1.04(r_g/r_1)^{1.99}$.

each parameter set, we performed 10 runs for different initial structures and obtained averaged values of r_g.

First, we focus on the collisions of aggregates consisting of 512 particles to see the influence of the material properties on the outcomes (Fig. 4*a*). We see that for $E_{\rm imp} \gtrsim 0.1E_{\rm roll}$ the gyration radius decreases with increasing impact energy irrespective of the material parameters. The slope (power-law index) of the decreasing portion is about -0.1. For $E_{\rm imp} \sim (0.1-1)n_kE_{\rm roll}$, r_g stays at a low value, indicating that compression of the aggregate ceases. This agrees with the criterion of maximum compression in the DT recipe. For $E_{\rm imp} \gtrsim (0.1-1)n_kE_{\rm roll}$, the aggregates are disrupted and $r_g/(r_1N_{\rm large}^{1/3})$ tends to scatter and increase with increasing $E_{\rm imp}$. This indicates that disrupted fragments are no longer compact compared to the maximum compressed aggregates.

Although the change in the gyration radius appears to have almost the same trend irrespective of the material properties, the data for high $\xi_{\rm crit}$ (e.g., $\xi_{\rm crit} = 30$ Å) deviate from the slope at relatively low $E_{\rm imp}$. This early deviation implies that the collisional aggregates are disrupted before being fully compressed. Material dependence of the degree of maximum compression will be discussed in § 3.2.

Figure 4*b* shows the dependence of r_g on the mass of aggregates. We find the same trend as that of 512 particles for large aggregates composed of 2048 and 8192 particles. Namely, r_g begins to decrease at $E_{\rm imp} \sim 0.1E_{\rm roll}$ and attains its minimum at $E_{\rm imp} \sim (0.1-1)n_kE_{\rm roll}$; the slope of r_g is also about -0.1. A difference appears in the absolute value of r_g, that is, r_g becomes large with increasing the number of particles in spite of the normalization by $r_1N_{\rm large}^{1/3}$.

In order to scale the absolute values of the gyration radius r_g, we change the normalization of r_g. Figure 5 shows r_g normalized by $r_1N_{\rm large}^{1/2.5}$ instead of $r_1N_{\rm large}^{1/3}$. With this normalization, our numerical results are completely scaled in the compression regime of $0.1E_{\rm roll} \lesssim E_{\rm imp} \lesssim 0.1n_kE_{\rm roll}$ for all $N_{\rm total}$, the sum of the number of particles of two colliding aggregates. The scaling law is expressed as

$$\frac{r_g}{r_1N^{1/2.5}} = \left(\frac{E_{\rm imp}}{0.15NE_{\rm roll}}\right)^{-0.10}, \tag{6}$$

where we use $n_k \simeq N_{\rm total}$ and set $N_{\rm large} = N_{\rm total} \equiv N$, because we deal with collisions in the compression regime without disruption.

We explain the scaling law from equation (6) in a similar way as in Wada et al. (2007). From 2D numerical simulations of aggregate collisions, we obtained a scaling law

$$\frac{r_g}{r_{g,\rm comp}} = \left(\frac{E_{\rm imp}}{bNE_{\rm roll}}\right)^{-\alpha}, \tag{7}$$

using a simple model illustrated in Figure 6. Here, α and b are constants. Equation (7) is applicable to 3D collisions as well. As seen in Figure 6, the compression begins at $E_{\rm imp} = b'E_{\rm roll}$ (b' is another constant) and r_g decreases from $r_{g,\rm BCCA}$, the gyration radius of initial BCCA clusters. As $E_{\rm imp}$ increases further, the compression ceases at $E_{\rm imp} = bNE_{\rm roll}$, where $r_g = r_{g,\rm comp}$. The exponent α is determined so that the line passes the point $(E_{\rm imp}, r_g) = (b'E_{\rm roll}, r_{g,\rm BCCA})$. Denoting the fractal dimension of the initial BCCA clusters ($\simeq 2$) by d_f and that of the aggregates compressed to the maximum extent by d_c, we have the gyration radii of them,

$$r_{g,\rm BCCA} \simeq r_1N^{1/d_f}, \tag{8}$$

$$r_{g,\rm comp} \simeq r_1N^{1/d_c}. \tag{9}$$

Then, the exponent α is given by

$$\alpha = \frac{1}{d_f} - \frac{1}{d_c}, \tag{10}$$

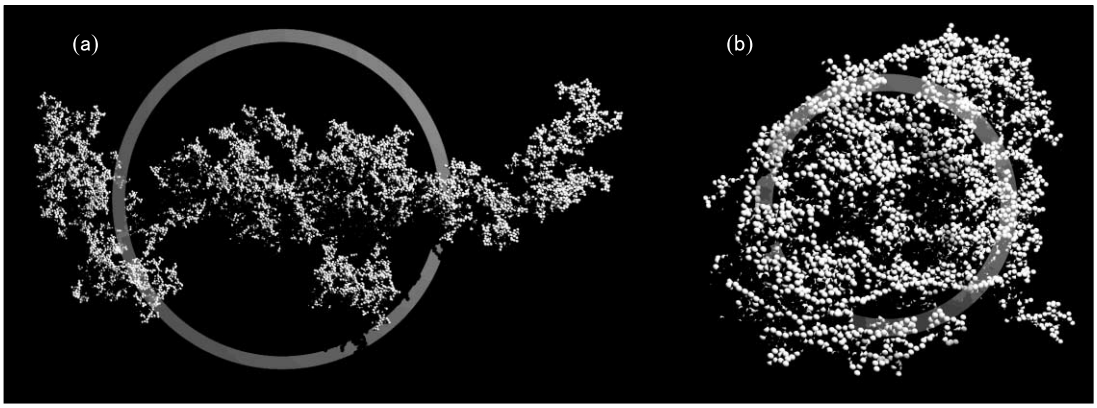

FIG. 3.—Examples of collisional outcomes: (*a*) no restructuring ($u_{\rm imp} = 0.024$ m s^{-1} and $E_{\rm imp} = 0.01E_{\rm roll}$) and (*b*) maximum compression ($u_{\rm imp} = 13$ m s^{-1} and $E_{\rm imp} = 0.19n_kE_{\rm roll}$). Both resultant aggregates are composed of 16,384 ice particles of 0.1 μm radius with $\xi_{\rm crit} = 8$ Å. The gray ring for each aggregate indicates the size of the gyration radius.

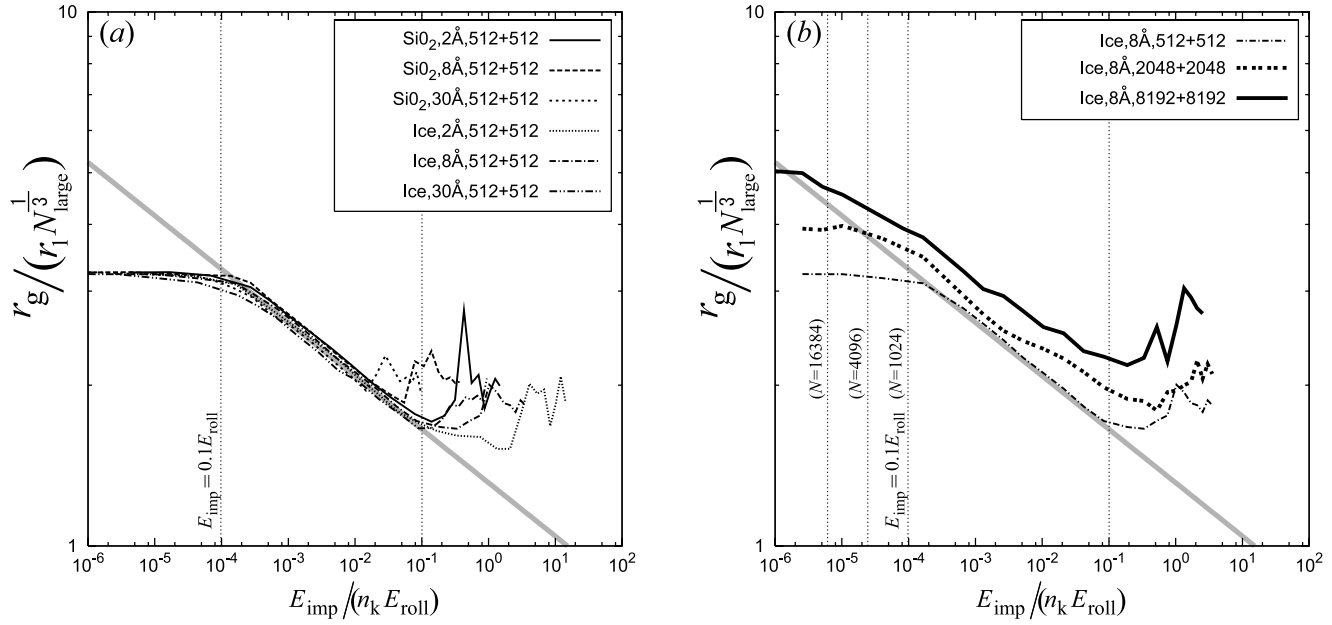

FIG. 4.—(*a*) Gyration radius of the largest fragment, r_g, as a function of the impact energy $E_{\rm imp}$. The vertical axis is r_g normalized by $r_1N_{\rm large}^{1/3}$. Each line corresponds to each parameter set: quartz or ice, $\xi_{\rm crit}=2$, 8, or 30 Å. In this figure, the number of particles of the aggregates before impact is fixed to $N_0=512$. The outputs are averaged over different initial aggregates produced by random numbers. The vertical dotted lines indicate $E_{\rm imp}=0.1E_{\rm roll}$ and $0.1n_kE_{\rm roll}$, from left to right. The gray line is a fitting line expressed by $r_g/(r_1N_{\rm large}^{1/3})=1.6[E_{\rm imp}/(0.15NE_{\rm roll})]^{-0.10}$ (see also eq. [14]). (*b*) Same as (*a*), but the results are plotted for ice aggregates of $N_0=512$, 2048, and 8192 and $\xi_{\rm crit}=8$ Å. The vertical dotted lines with labels indicate $E_{\rm imp}=0.1E_{\rm roll}$ for $N=1024$, 4096, and 16,384.

where we assume $b'=b$ referring to the numerical results (see Fig. 5). Then, the line of r_g is expressed as

$$\frac{r_g}{r_1N^{1/d_c}}=\left(\frac{E_{\rm imp}}{bNE_{\rm roll}}\right)^{-\alpha}. \tag{11}$$

In the previous 2D simulations, we obtained $\alpha=1/1.57-1/d_c=0.137$, which implies $d_c\simeq 2$ for 2D compressed aggregates (Wada et al. 2007). On the other hand, comparing equations (6) and (11), we have $\alpha=0.10$, $b=0.15$, and $d_c\simeq 2.5$ in the present 3D simulations. The result of $d_c\simeq 2$ in the 2D simulation indicates that 2D aggregates can be compressed to the limit. On the other hand, 3D aggregates are not compressed to the limiting value of $d_c=3$. Indeed, Figure 5 shows that the gyration radii of compressed aggregates are distributed above the line of $\alpha=1/6$ (i.e., corresponding to $d_c=3$), indicating that it is hard to compress 3D aggregates to the limit. This analysis suggests that 3D aggregates maintain a relatively fluffy structure of $d_c\simeq 2.5$ even if they are compressed to the maximum extent by collisions.

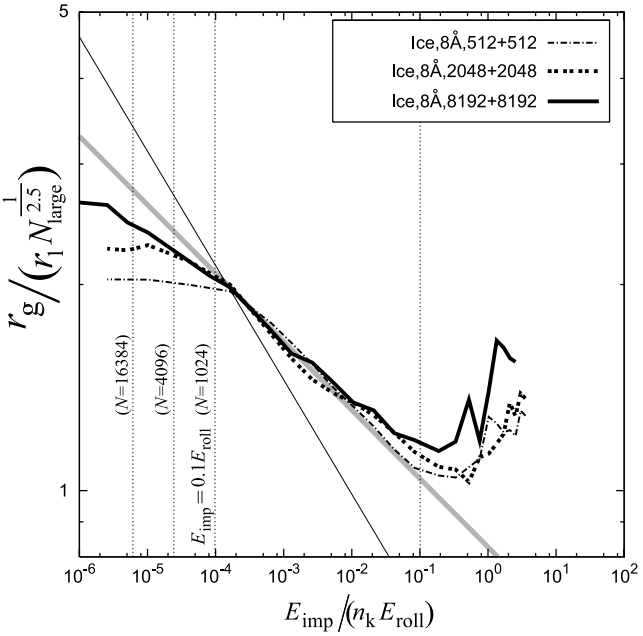

FIG. 5.—Same as Fig. 4*b*, but the vertical axis is r_g normalized by $r_1N_{\rm large}^{1/2.5}$. The gray line is a fitting line expressed by $r_g/(r_1N_{\rm large}^{1/2.5})=[E_{\rm imp}/(0.15NE_{\rm roll})]^{-0.10}$. The thin solid line is the one for $d_c=3$ and is expressed by $r_g/(r_1N_{\rm large}^{1/2.5})=9.8\times 10^{-3}[E_{\rm imp}/(0.15NE_{\rm roll})]^{-0.167}$.

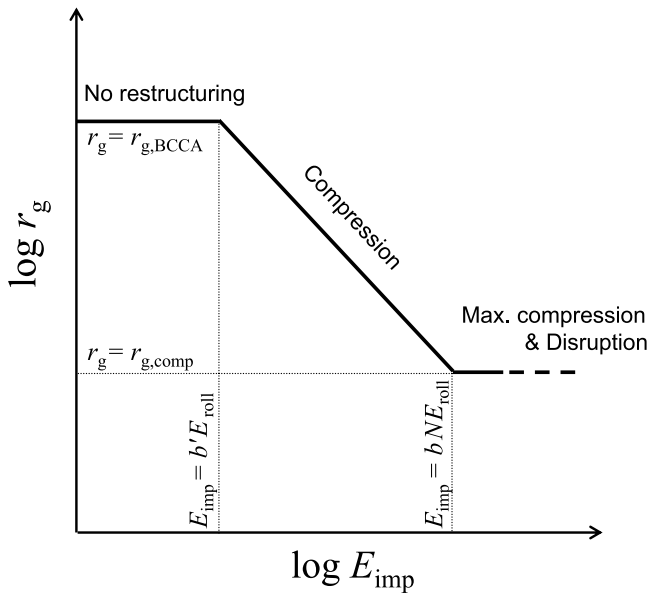

FIG. 6.—Schematic illustration of the change in the gyration radius r_g as a function of the impact energy $E_{\rm imp}$. BCCA clusters with $r_g=r_{g,\rm BCCA}$ begin to be compressed at $E_{\rm imp}=b'E_{\rm roll}$ and their compressions end at $E_{\rm imp}=bNE_{\rm roll}$, where b' and b are constants. We assume $b'\simeq b$ referring to the numerical results (Fig. 5).

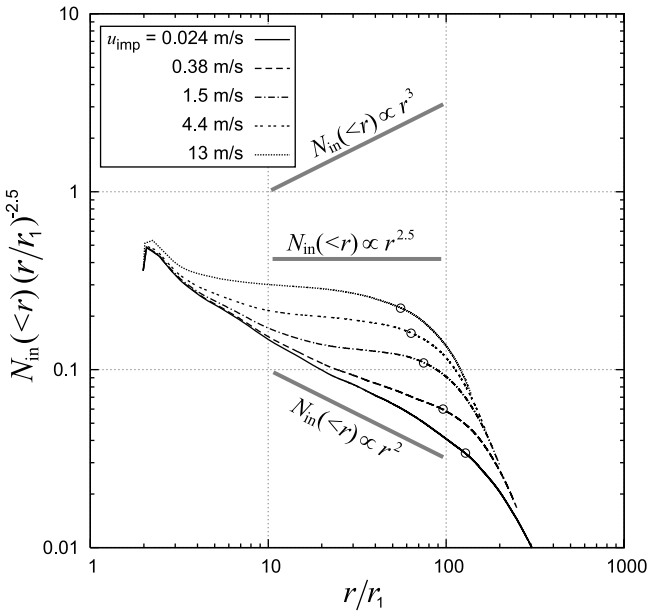

FIG. 7.—Number of particles $N_{in}(<r)$ within a distance r in the resultant aggregates of $N = 16,384$; $N_{in}(<r)$ normalized by $(r/r_1)^{2.5}$ are plotted as a function of r/r_1 for various impact velocities u_{imp} that do not cause aggregate disruption. In counting $N_{in}(<r)$, we first set the origin at the center of a particle in the aggregate and then take the average of $N_{in}(<r)$ after changing the origins to the centers of all the particles. We also take the average of the results for all collisions of initial BCCA clusters composed of 8192 particles. The circles plotted on the lines indicate the mean gyration radii. The slopes of the gray lines -0.5, 0, and 0.5 correspond to the fractal dimensions of 2, 2.5, and 3, respectively.

To confirm this result, we examine the number of particles $N_{in}(<r)$ within a distance r inside aggregates created in our simulation. By taking each particle's center as an origin of measuring the distance r, we count $N_{in}(<r)$ for all particles and average $N_{in}(<r)$. Figure 7 plots $N_{in}(<r)$ divided by $r^{2.5}$ as a function of r, indicating that $N_{in}(<r) \propto r^{2.5}$ if the slope is horizontal and $N_{in}(<r) \propto r^2$ if the slope is -0.5. When u_{imp} is too low to restructure the aggregates, they maintain initial BCCA structures of $d_f = 2$ without restructuring and result in the slope -0.5. With an increase in u_{imp}, the aggregates are compressed and the slope approaches horizontal in the region of large r, namely, from large-scale structures. For $u_{imp} \simeq 13$ m s^{-1}, the aggregates are compressed to the maximum extent, and the slope is almost horizontal for $5r_1 \lesssim r \lesssim r_g$. This means that the aggregates still have a fluffy structure with a fractal dimension $\sim$2.5. Furthermore, the aggregates that are not yet fully compressed also appear to have a fluffy structure with a fractal dimension $\sim$2.5 if we focus on the relatively large-scale structure. The same results are obtained for the other N. Therefore, we conclude that aggregates compressed to the maximum extent still have a relatively fluffy structure with their fractal dimension $d_c \simeq 2.5$.

Introducing the specific energy ϵ_{imp}, the impact energy per particle defined by

$$\epsilon_{imp} \equiv \frac{E_{imp}}{N}, \tag{12}$$

equation (11) is written as

$$\frac{r_g}{r_1 N^{1/d_c}} = \left(\frac{\epsilon_{imp}}{bE_{roll}}\right)^{-\alpha}. \tag{13}$$

Note that ϵ_{imp} is independent of N, so that the right-hand side of equation (13) is independent of N. Equation (13) is a scaling law of the gyration radius of aggregates compressed by collisions in terms of the specific impact energy ϵ_{imp}. Equation (13) is expressed by

$$\frac{r_g}{r_1 N^{1/3}} = \left(\frac{\epsilon_{imp}}{bE_{roll}}\right)^{-\alpha} N^{1/d_c - 1/3} \tag{14}$$

as well. The N-dependence in Figure 4*b* that $r_g/(r_1 N^{1/3})$ increases with N is explained quantitatively by this relation.

3.2. *The Number of Contacts*

The number of contacts per particle in an aggregate, n_{con}, is another measure of aggregate compression; n_{con} increases as an aggregate is compressed. Figure 8*a* shows that n_{con} (of the largest fragment) increases with increasing impact energy E_{imp}. When

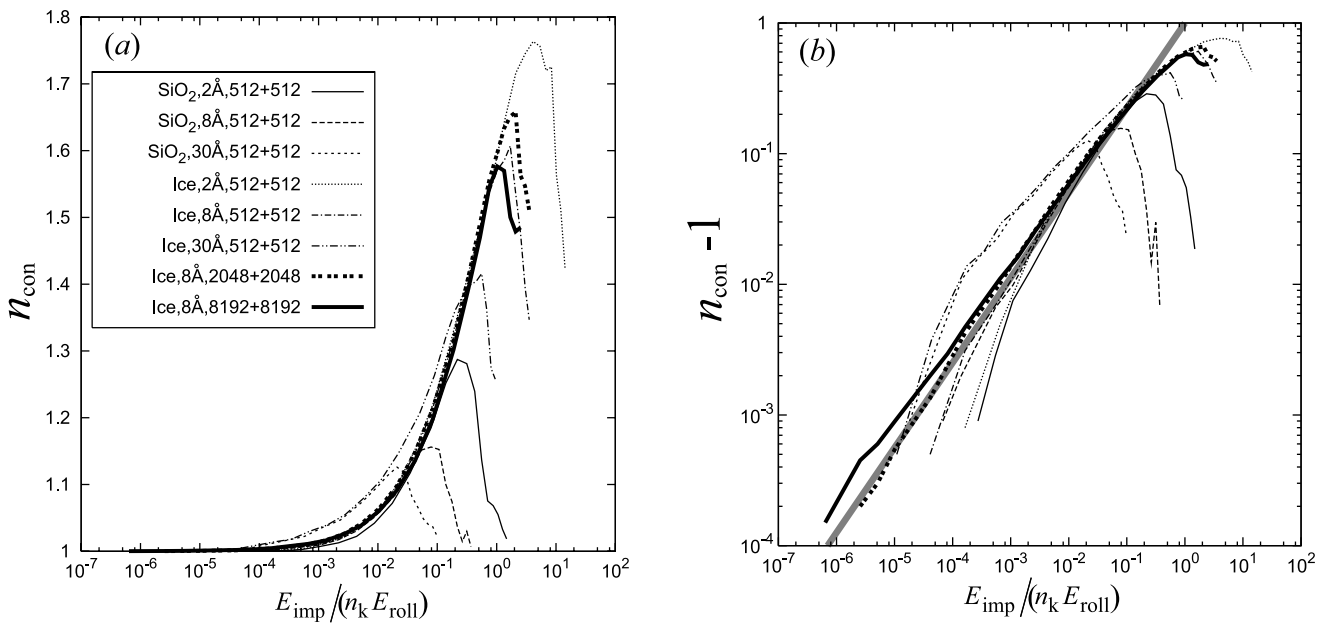

FIG. 8.—(*a*) Number of contacts n_{con} per particle in the largest fragment after impact vs. impact energy E_{imp}. The simulation setting for each line is the same as in Fig. 4. (*b*) Same as (*a*), but a log-log plot of $n_{con} - 1$ vs. $E_{imp}/(n_k E_{roll})$. The gray line is expressed by $n_{con} - 1 = [E_{imp}/(n_k E_{roll})]^{0.65}$.

TABLE 3
CRITICAL DISPLACEMENT ξ_{crit} FOR ROLLING AND CHARACTERISTIC ENERGIES

Material	ξ_{crit} (Å)	$E_{roll}/(F_c\delta_c)$	$E_{break}/(F_c\delta_c)$	E_{roll}/E_{break}
Ice.....	2	2.98	1.54	1.94
	8	11.9	1.54	7.73
	30	44.8	1.54	29.1
Quartz.....	2	28.7	1.54	18.6
	8	115	1.54	74.7
	30	430	1.54	279

E_{imp} is smaller than E_{roll}, n_{con} hardly increases from that of the initial BCCA clusters ($n_{con} \simeq 1$), indicating practically no restructuring. When $E_{imp} \gtrsim E_{roll}$, n_{con} increases with E_{imp} through restructuring of the aggregate due to rolling. The trend of n_{con} is almost irrelevant to ξ_{crit}, particle materials, and N_{total}, implying that n_{con} is scaled by $n_k E_{roll}$. For $\xi_{crit} = 30$ Å, however, n_{con} is slightly larger than those for smaller ξ_{crit}. This may reflect the fact that particles with high ξ_{crit} have a large possibility to be in contact with their neighbor particles, because they can roll large distances without energy dissipation compared to those with low ξ_{crit}. Figure 8*b* shows that n_{con} is expressed as

$$n_{con} - 1 = \left(\frac{E_{imp}}{n_k E_{roll}}\right)^{0.65} \quad (15)$$

for $E_{imp} \lesssim 0.1 n_k E_{roll}$. A similar relation with the power index of 0.75 was found in our 2D simulations (Wada et al. 2007). Figure 8*b* also shows that n_{con} begins to deviate from equation (15) when the impact energy attains $\sim n_k E_{break}$. This is due to disruption of the aggregates. The degree of maximum compression depends on the ratio E_{roll}/E_{break} as discussed in the 2D simulations (see Fig. 8 and Table 3). For small E_{roll}/E_{break} such as ice aggregates with $\xi_{crit} = 2$ Å, particles can be rolled a lot while keeping their contacts, so aggregates can be compact. In contrast, for a large E_{roll}/E_{break} such as quartz with $\xi_{crit} = 30$ Å, the aggregates break before becoming compact. The ratio E_{roll}/E_{break} represents the difficulty of restructuring and compression as seen in our 2D simulations (Wada et al. 2007).

3.3. *The Largest Fragment Size at Collisional Disruption*

Figure 9 shows the ratio N_{large}/N_{total} as a function of the impact energy E_{imp} normalized by $n_k E_{break}$ for collisions of aggregates with various parameter sets. The degree of disruption is expressed by this ratio N_{large}/N_{total}. A small N_{large}/N_{total} ratio means intense disruption of aggregates. We term the cases of $N_{large}/N_{total} \leq 0.5$ catastrophic disruptions. We see that fragmentation begins at $E_{imp} \simeq 3 n_k E_{break}$. Catastrophic disruption occurs at $E_{imp} \gtrsim 10 n_k E_{break}$. These results are in agreement with the DT recipe that the disruption process would be scaled by $n_k E_{break}$. However, there seems to be a tendency for quartz aggregates to be disrupted easier than ice. This tendency is also seen in our 2D simulations (Wada et al. 2007). The critical velocities for catastrophic disruption, corresponding to $E_{imp} = 10 n_k E_{break}$, are $\sim 34\ m\ s^{-1}$ ($\sim 3.4\ m\ s^{-1}$) for the ice (quartz) aggregates with a particle radius of 0.1 μm. On the other hand, experimental studies (Poppe et al. 2000; Blum & Wurm 2000; Wurm et al. 2005) suggested that the critical velocity was much higher than that of the present results by an order of magnitude. The reason for the difference in the critical velocity remains unclear so far.

In Figure 9, the degree of disruption is shown to be almost independent of the aggregate size N_{total}, while in our 2D simulation, aggregates tend to be harder against disruption with increasing N_{total} (Wada et al. 2007). However, detailed inspection shows that disruption occurs slightly easier for $N_{total} = 16,384$ than for $N_{total} \leq 4096$. This may be dependent on the initial structure (and collision direction) of aggregates. If the collision cross section is large, disruption occurs at many points widely distributed in the aggregates and they tend to split into several fragments. The influence of the initial structure for large aggregates is also observed in our 2D simulation, but is weaker in the 3D simulation than in the 2D. The size dependence on the degree of disruption would not be important for 3D aggregate collisions.

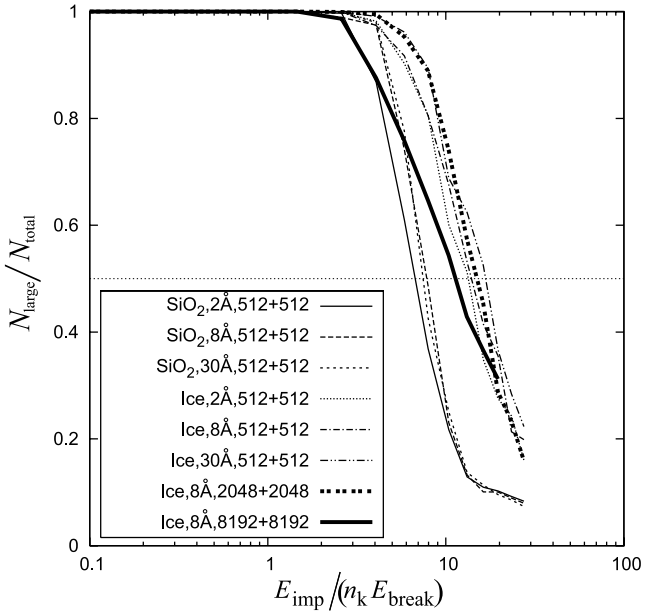

FIG. 9.—Ratio of the number of particles in the largest fragment, N_{large}, to the total number of particles, N_{total}, as a function of the impact energy E_{imp}. The simulation setting for each line is the same as that shown in Fig. 4.

3.4. *Mass Distribution of Fragments*

Figure 10 shows cumulative mass distributions of fragments produced by disruption of aggregates for various impact velocities, namely, the number of fragments heavier than a given mass. We plot the mass distributions for the collisions of aggregates consisting of 8192 particles, by averaging the results of 10 runs to make the resolution as high as possible. At low impact velocities the distributions are almost flat, because low-velocity collisions produce only a few small fragments. A large number of fragments are produced with increasing impact velocity, so that the mass distributions tend to approach a power law. The distributions seem to be expressed by two power laws having the slope ~ -2 for small fragments ($\lesssim 10$ particles) and ~ -0.5–1 for relatively large fragments ($\gtrsim 10$ particles). Such distributions indicate that there remain a few large fragments, while a large number of small fragments are produced by the collisions for the impact energies $E_{imp} < 20 n_k E_{break}$. The distribution may be represented by a single power law for collisions with $E_{imp} \gg 20 n_k E_{break}$. Collision simulations for higher velocity and the larger clusters are required for more thorough discussion.

4. PRESSURE OF AGGREGATES

In this section we develop a macroscopic description of aggregate compression by introducing the internal "pressure" of aggregates. We determine the pressure of aggregates based on the obtained scaling law of the gyration radius. In our numerical

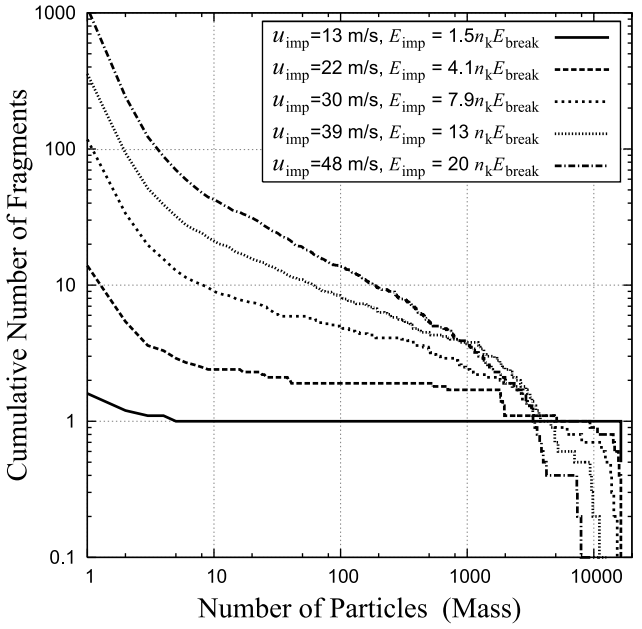

FIG. 10.—Mass distributions of fragments produced by disruption at collisions of aggregates consisting of 8192 particles. The vertical axis represents the cumulative number of fragments heavier than a given mass (i.e., the number of particles). The plotted data are averaged over 10 runs for each impact velocity.

results, the gyration radius r_g, or the volume V, of the resultant aggregate decreases with increasing impact energy $E_{\rm imp}$. We assume that the dependence of V on $E_{\rm imp}$ is described by the relation given by

$$dE_{\rm imp} = -P\,dV. \tag{16}$$

The coefficient P can be regarded as the "pressure" (or the strength) of the aggregate. Exactly speaking, since the impact energy is dissipated irreversibly in aggregate compression, P is not a usual pressure and is a measure of strength of the aggregate against compression at the impact. In the present paper, however, we call P the pressure of aggregates for convenience. If the pressure is expressed as a function of the bulk density ρ of an aggregate, we obtain an "equation of state" (EOS) of an aggregate, which is applicable to the description of aggregate compression. The volume of an aggregate is approximately given by

$$V \sim r_g^3. \tag{17}$$

We also define the specific volume of an aggregate as $v \equiv V/N$. From the scaling law of the gyration radius (eq. [13]), v is proportional to $\epsilon_{\rm imp}^{-3\alpha} N^{-(1-3/d_c)}$, where $\epsilon_{\rm imp} = E_{\rm imp}/N$ is the impact energy per particle. That is, the specific volume is not an "intensive variable" but depends on N. Using equation (16), we obtain P as

$$P = -\frac{d\epsilon_{\rm imp}}{dv} \propto v^{-(3\alpha+1)/(3\alpha)} N^{(3-d_c)/(3\alpha d_c)}. \tag{18}$$

This indicates that P is not an intensive variable, either. For a macroscopic description of aggregate compression, the pressure and the specific volume should be intensive variables as they are in the usual thermodynamics. To make the specific volume and the pressure intensive variables, we introduce a new concept of volume having the dimension of length to the power d_c as is seen in § 4.1.

4.1. *Equation of State in Terms of the Fractal Variables*

For an aggregate with a characteristic radius r_c (Mukai et al. 1992) and a fractal dimension d_c, we define its "fractal volume" V_f by

$$V_f \equiv A r_c^{d_c}. \tag{19}$$

The coefficient A is given by

$$A = \frac{\pi^{d_c/2}}{\Gamma(1 + d_c/2)}, \tag{20}$$

for a spherical aggregate of the fractal dimension d_c, where $\Gamma(z)$ is the Γ-function. For $d_c = 2.5$, A is 3.69, slightly less than $4\pi/3$ for a 3D compact sphere. For a homogeneous sphere with radius r_c, the gyration radius r_g is given by

$$r_g^2 = \frac{\int r^2\,dV_f'}{\int dV_f'} = \frac{\int_0^{r_c} r^2 r^{d_c-1}\,dr}{\int_0^{r_c} r^{d_c-1}\,dr} = \frac{d_c}{d_c+2} r_c^2, \tag{21}$$

where $V_f' \equiv A r^{d_c}$. Eliminating r_c from equations (19) and (21), the fractal volume is expressed as

$$V_f = V_{f,1} \left(\frac{r_g}{r_1}\right)^{d_c}, \tag{22}$$

where $V_{f,1} = A(r_1[(d_c+2)/d_c]^{1/2})^{d_c}$. Since r_g is proportional to N^{1/d_c} according to the scaling law from equation (13), V_f is proportional to N. Thus, V_f is an extensive variable. Using equation (22), the specific fractal volume (i.e., the fractal volume per particle) v_f is given by

$$v_f \equiv \frac{V_f}{N} = V_{f,1} \left(\frac{r_g}{r_1 N^{1/d_c}}\right)^{d_c}. \tag{23}$$

Substituting the scaling law from equation (13) into the above equation, we have

$$v_f = V_{f,1} \left(\frac{\epsilon_{\rm imp}}{bE_{\rm roll}}\right)^{-(d_c-d_f)/d_f}, \tag{24}$$

where $b = 0.15$ (see § 3.1). Note that v_f is an intensive variable. The fractal density of an aggregate, ρ_f, is defined by

$$\rho_f \equiv \frac{m_1 N}{V_f} = \frac{m_1}{v_f} = \rho_{f,1} \left(\frac{r_g}{r_1 N^{1/d_c}}\right)^{-d_c} = \rho_{f,1} \left(\frac{\epsilon_{\rm imp}}{bE_{\rm roll}}\right)^{(d_c-d_f)/d_f} \tag{25}$$

with

$$\rho_{f,1} = \frac{m_1}{V_{f,1}}. \tag{26}$$

The fractal density is also an intensive variable.

Defining the "fractal pressure" of an aggregate, P_f, by

$$d\epsilon_{\rm imp} = -P_f\,dv_f \tag{27}$$

in analogy to equation (16), we obtain

$$P_f = -\frac{d\epsilon_{\rm imp}}{dv_f} = \frac{d_f}{d_c - d_f}\frac{bE_{\rm roll}}{V_{f,1}}\left(\frac{v_f}{V_{f,1}}\right)^{-d_c/(d_c-d_f)} \quad (28)$$

from equation (24). Note that P_f is an intensive variable because v_f is intensive. It should be noted that the dimension of P_f is not N m^{-2}. The fractal pressure is also expressed in terms of ρ_f as

$$P_f = \frac{d_f}{d_c - d_f}\frac{bE_{\rm roll}\rho_{f,1}}{m_1}\left(\frac{\rho_f}{\rho_{f,1}}\right)^{d_c/(d_c-d_f)} \quad (29)$$

from equations (25) and (26). We call equation (29) the "EOS of an aggregate." For $d_f = 2$ and $d_c = 2.5$, the EOS is reduced to

$$P_f = 4\frac{bE_{\rm roll}\rho_{f,1}}{m_1}\left(\frac{\rho_f}{\rho_{f,1}}\right)^5. \quad (30)$$

Equations (28) and (29) are equivalent to the scaling law from equation (13).

4.2. *Comparison with Other Equations of State*

Using the volume and the density of an aggregate given by

$$V = \frac{4}{3}\pi r_c^3 = \frac{4}{3}\pi\left(\sqrt{\frac{5}{3}}r_g\right)^3, \quad \rho = \frac{m_1 N}{V}, \quad (31)$$

instead of the fractal volume and the fractal density, we can derive an expression of the pressure in the ordinary sense. Here we set $d_f = 2$ and $d_c = 2.5$. As described in the Appendix, the ordinary pressure P of an aggregate is given by

$$P = -\frac{dE_{\rm imp}}{dV} = \frac{10}{3}\left(\frac{3}{5}\right)^{-5}\frac{bE_{\rm roll}\rho_m}{m_1}\left(\frac{\rho}{\rho_m}\right)^{13/3}N^{2/3}, \quad (32)$$

where ρ_m is the material density. As shown above, P depends not only on the density ρ of the aggregate but also on its size N. Figure 11 plots the P-ρ relation given by equation (32) for various N, where the upper limit of ρ corresponding to the maximum compression [$r_g/(r_1 N^{1/d_c}) = 1$] is given by (see Appendix)

$$\rho_{\rm max} = \left(\frac{3}{5}\right)^{3/2}\rho_m N^{-1/5}. \quad (33)$$

Sirono & Greenberg (2000) analytically obtained the compressive and the tensile strengths of aggregates as a function of the relative density $\hat{\rho} = \rho/\rho_m$. They considered aggregates consisting of periodically connected particle chains. The interaction between particles in contact is the same as those used in the present paper. According to them, the compressive strength $P_{\rm SG}$ is determined by the rolling resistance when the relative density is low ($\hat{\rho} \lesssim 0.3$) and is given by

$$P_{\rm SG} = \frac{24\pi\gamma r_1 \xi_{\rm crit}(N_c - 1)}{l^2(l - 2r_1)(N_c - 3)} \quad (34)$$

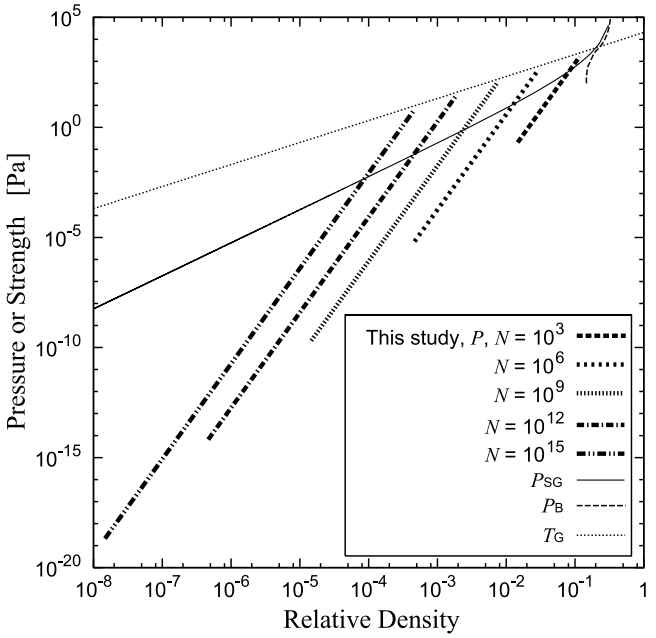

FIG. 11.—Pressure, compressive strength, and tensile strength of aggregates as a function of relative density ρ/ρ_m. The thick dashed and dotted lines represent the pressure P for various N formulated in this study (eq. [32]). The solid line $P_{\rm SG}$ is the theoretical compressive strength given by Sirono & Greenberg (2000). The thin dashed line $P_{\rm B}$ is the compressive strength of aggregates composed of spherical SiO_2 particles measured by Blum et al. (2006). The thin dotted line $T_{\rm G}$ is the tensile strength given by Greenberg et al. (1995). Here, we assumed aggregates consisting of ice particles of $r_1 = 0.1$ μm and $\xi_{\rm crit} = 2$ Å.

with

$$\hat{\rho} = \frac{4\pi r_1^3(3N_c - 5)}{3l^3}, \quad (35)$$

where N_c is the number of particles of radius r_1 constituting a chain of length l. The relation between N_c and l is given by

$$N_c = \sqrt{\left(\frac{l}{2r_1} - 1\right)^2 + \left(\frac{l}{2r_1}\right)^2} + 1. \quad (36)$$

Since we focus on very fluffy aggregates of $\hat{\rho} < 0.1$, we plot $P_{\rm SG}$ given by equation (34) for $r_1 = 0.1$ μm, $\gamma = 100$ mJ m^{-2}, and $\xi_{\rm crit} = 2$ Å in Figure 11. Aggregates consisting of particle chains are expected to be strong against compression, because the force in the direction of particle connection can be well supported by the chains. In consequence, the pressure P obtained from our numerical simulations is lower than $P_{\rm SG}$ in most ranges of $\hat{\rho}$. Blum et al. (2006) experimentally measured the compressive strength of aggregates produced by random ballistic deposition of SiO_2 spheres of radius 0.76 μm. The relative density of their aggregates is higher than $\sim$0.15. The compressive strength $P_{\rm B}$ that they measured is also plotted in Figure 11. For high density ($\gtrsim$0.2), $P_{\rm B}$ is close to $P_{\rm SG}$ and P derived theoretically. For low density, on the other hand, there is a lack of experimental data, and thus, experiments in these densities are strongly encouraged to compare with our results.

One may expect that the upper limit of P is close to the tensile strength of aggregates, because they are disrupted when the pressure exceeds their tensile strength. Greenberg et al. (1995) evaluated

the tensile strength T_G of an aggregate to be a total adhesive energy per unit volume of the aggregate and obtained

$$T_G = \frac{n_{con} N E_{break}}{V} = \frac{n_{con} E_{break} \rho_m}{m_1} \frac{\rho}{\rho_m}, \quad (37)$$

where E_{break} is regarded as the adhesive energy per pair of particles in contact. The T_G-ρ relation is plotted in Figure 11 for ice aggregates with $n_{con} = 1.5$, which is approximately the maximum value derived from our numerical simulations (see Fig. 8 in § 3.2). In Figure 11, P is always less than T_G for all N, although P may slightly exceed T_G for a higher value of E_{roll}. The pressure of aggregates, therefore, has a limit around their tensile strength given by equation (37), indicating that aggregates are compressed without disruption until P equals T_G as shown by Sirono (2004).

In summary, the present P-ρ relation describes compression of a fluffy dust aggregate in a wide range of pressures. When the density of aggregates is low enough, the pressure P of the aggregates is smaller than P_{SG}, because initial BCCA clusters and their slightly restructured ones are much more fragile than regularly arranged particle chains. For well-compressed aggregates, P becomes larger than P_{SG}, because the number of contacts n_{con} becomes larger than that of the chain structure for which $n_{con} \simeq 1$. Increases in P and ρ stop when $P \simeq T_G$, since disruption prevents aggregates from further compression.

4.3. *Description of Aggregate Compression with the Fractal Pressure*

In § 4.2 we derived the EOS of aggregates compressed by an impact with E_{imp} large enough to restructure and compress the aggregates. We show that the fractal pressure given by equation (28) also reproduces the r_g-E_{imp} relation (Fig. 5) in the lowest E_{imp} region of no restructuring.

Consider an initial BCCA cluster of specific fractal volume $v_{f,BCCA}$ compressed by a collision with specific energy ϵ_{imp}. In view of equation (27), we assume that the resultant specific fractal volume v_f is determined by

$$\int_0^{\epsilon_{imp}} d\epsilon'_{imp} = -\int_{v_{f,BCCA}}^{v_f} P_f(v'_f) dv'_f. \quad (38)$$

Substituting P_f given by equation (28) into equation (38) and integrating both sides, we have

$$\frac{\epsilon_{imp}}{bE_{roll}} = \left(\frac{v_f}{V_{f,1}}\right)^{-d_f/(d_c-d_f)} - \left(\frac{v_{f,BCCA}}{V_{f,1}}\right)^{-d_f/(d_c-d_f)}. \quad (39)$$

Using equations (8) and (23), we obtain the gyration radius as a function of ϵ_{imp} to be

$$\frac{r_g}{r_1} = \left(\frac{1}{N} + \frac{\epsilon_{imp}}{bE_{roll}}\right)^{-(1/d_f - 1/d_c)} N^{1/d_c}. \quad (40)$$

It is readily seen that equation (40) is an extension of the scaling law from equation (13). In Figure 12 we plot equation (40) for $N = 1024, 4096$, and 16,384 with $b = 0.15$ (see § 3.1). Note that equation (40) reproduces the numerical results fairly well even for the energy range of $0 \le E_{imp} \lesssim E_{roll}$. Therefore, the EOS is applicable to a wide range of the impact energy so long as the disruption does not occur. The validity of equation (38) will be examined by Suyama et al. (2008), who directly calculate growth of aggregates by successive collisions.

Recently, Ormel et al. (2007) modeled a change in the volume of aggregates at collisions. They introduced the enlargement

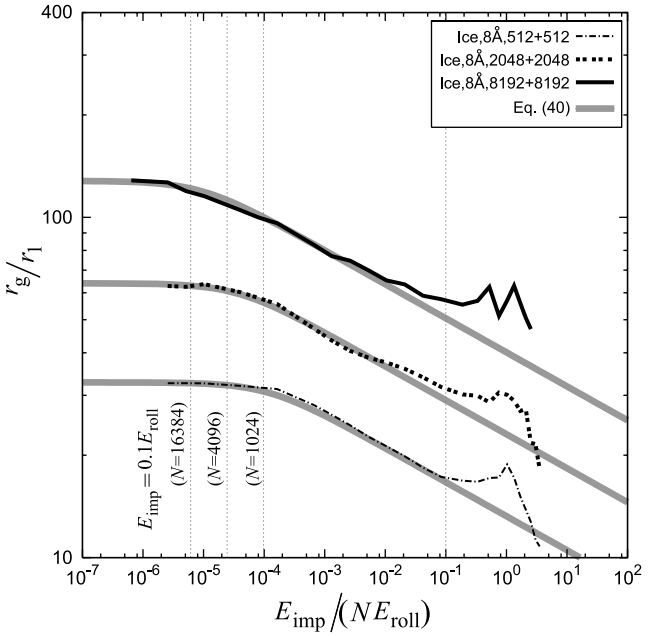

FIG. 12.—Gyration radius r_g of the largest fragment as a function of impact energy E_{imp}. The gray lines represent eq. (40) for $N = 1024$, 4096, or 16,384, under the condition of $d_f = 2$, $d_c = 2.5$, and $b = 0.15$.

parameter Ψ defined by $\Psi = V/V^*$. Here, V is the aggregate volume that reproduces its geometrical cross section, and V^* is the volume if the aggregate is closely packed. We take $V = 4\pi r_g^3/3$ to compare their model with our numerical results and $V^* = 4\pi r_1^3 N/3$ (a factor 1/0.74 should multiply this if one considers close packing). Then, Ψ is expressed by

$$\Psi = \left(\frac{r_g}{r_1}\right)^3 \frac{1}{N}. \quad (41)$$

Following Ormel et al. (2007) we calculate the change in r_g for a collision of two identical BCCA clusters of mass $N/2$, with $d_f = 2$ and the enlargement parameter Ψ_1 as follows. If the impact energy E_{imp} is less than E_{roll}, a hit-and-stick collision occurs, and the fractal dimension of the resultant aggregate is unchanged. For $E_{imp} \ge E_{roll}$, Ormel et al. (2007) assume that the degree of compression of aggregates due to collisions scales linearly with E_{imp}, and the enlargement parameter Ψ changes with E_{imp} as

$$\Psi - 1 = \left(1 - \frac{E_{imp}}{NE_{roll}}\right)(\Psi_1 - 1). \quad (42)$$

Given the gyration radius of the aggregates before collision, $r_{g,BCCA,1} = r_1(N/2)^{1/d_f}$, equations (41) and (42) yield r_g of the resultant aggregate. The model of Ormel et al. (2007) gives

$$\frac{r_g}{r_1} = \begin{cases} N^{1/d_f}, & E_{imp} < E_{roll}, \\ N^{1/3}\left\{1 + \left(1 - \dfrac{E_{imp}}{NE_{roll}}\right)\left[\left(\dfrac{N}{2}\right)^{(3-d_f)/d_f} - 1\right]\right\}^{1/3}, & E_{imp} \ge E_{roll}, \end{cases} \quad (43)$$

which is plotted in Figure 13 for $N = 1024$, 4096, and 16,384 with $d_f = 2$. Each line has a discontinuity at $E_{imp} = E_{roll}$, because

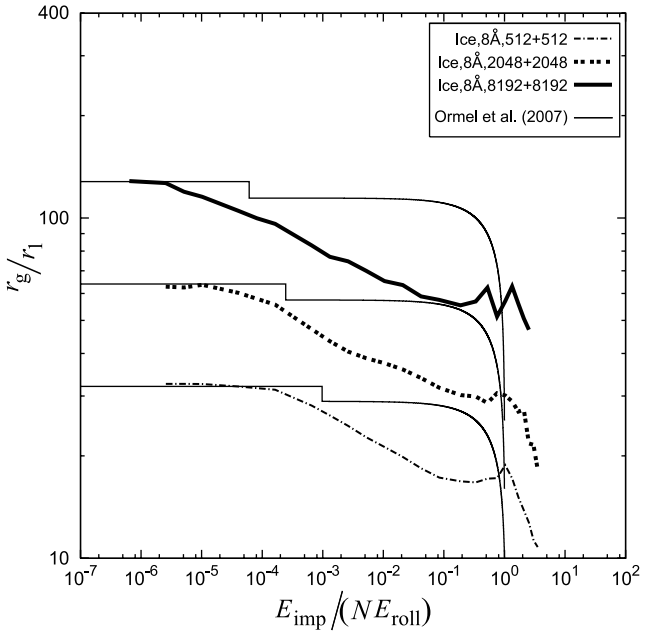

FIG. 13.—Comparison of the gyration radius r_g given by our numerical results and by a model of Ormel et al. (2007). Gyration radius r_g of the largest fragment is plotted as a function of impact energy $E_{\rm imp}$. The three solid lines indicate r_g based on the model of Ormel et al. (2007; eq. [43] in the text) for $N = 1024$, 4096, and 16,384.

Ormel et al. (2007) neglected newly created empty space produced at the moment of sticking for $E_{\rm imp} \geq E_{\rm roll}$. Figure 13 shows that the model of Ormel et al. (2007) gives a much lower degree of compression than that of our numerical results for $E_{\rm roll} \lesssim E_{\rm imp} \lesssim NE_{\rm roll}$. This is due to the assumption that the compression proceeds linearly with impact energy. Around $E_{\rm imp} \sim NE_{\rm roll}$, r_g given by the model of Ormel et al. (2007) rapidly decreases to the minimum $r_1 N^{1/3}$, which is much less than that of our numerical results. The difference in the degree of maximum compression can be resolved if V^* is replaced by the volume at the maximum compression, $4\pi(r_1 N^{1/d_c})^3/3$.

The collision cross section σ is used to solve a coagulation equation for growth of dust aggregates using the coagulation equation (see Blum 2006 for a review). Several kinds of "radii" of an aggregate are proposed as a representative of aggregate size, such as, toothing radius and geometrical radius (Ossenkopf 1993; Ormel et al. 2007). Here, we use the gyration radius r_g as a representative of the aggregate size, because we already have the useful scaling formula of gyration radius (eq. [40]). Because of the limitations of our numerical simulations, we give the collision cross section σ under the following assumptions: (1) the mass distribution of aggregates is monodisperse and (2) the r_g of the resultant aggregates are given by equation (40) including offset collisions. Then, the collision cross section is given by

$$\sigma = \pi(2r_g)^2 = 4\pi r_1^2 \left(\frac{1}{N} + \frac{m_1 u_{\rm imp}^2}{8bE_{\rm roll}}\right)^{-2(1/d_f - 1/d_c)} N^{2/d_c}. \quad (44)$$

To obtain the cross section applicable to a wide range of conditions, it is necessary to study the collisions of aggregates of different sizes and structures and arbitrary offset collisions.

5. SUMMARY

We carried out numerical simulations of head-on collisions of 3D BCCA clusters to study the compression and disruption processes in their growth. We used the numerical code developed in our previous study (Wada et al. 2007) and examined the collisions of 3D BCCA clusters composed of 512, 2048, and 8192 particles.

The compression process is represented by changes in the gyration radius r_g and the number of contacts of aggregates $n_{\rm con}$. The gyration radius of BCCA clusters (with the fractal dimension $d_f \simeq 2$) decreases with increasing impact energy, reflecting aggregate compression. We obtained a scaling law for the gyration radius of the compressed aggregate as (for $E_{\rm imp} \lesssim bNE_{\rm roll}$)

$$r_g = r_1 N^{1/d_c} \left(\frac{1}{N} + \frac{E_{\rm imp}}{bNE_{\rm roll}}\right)^{-(1/d_f - 1/d_c)}, \quad (45)$$

where d_c is its fractal dimension and $b \simeq 0.15$. This holds irrespective of both material properties and the critical rolling displacement $\xi_{\rm crit}$. The scaling law is confirmed by the numerical result that the compressed aggregates, even not fully compressed, appear to have a fractal structure with a fractal dimension d_c if we focus on relatively large-scale structure. Maximum compression occurs when the impact energy is nearly equal to the energy necessary to roll all contacts, $E_{\rm imp} \sim (0.1-1)n_k E_{\rm roll}$. This is consistent with the results of 2D simulations performed by Wada et al. (2007) and Dominik & Tielens (1997). The compressed aggregates have a fractal structure with $d_c \simeq 2.5$, suggesting that 3D dust aggregates remain a relatively fluffy structure even if they are compressed to a maximum extent by collisions. For the number of contacts per particle, we also obtain an empirical relation as (for $E_{\rm imp} \lesssim n_k E_{\rm break}$)

$$n_{\rm con} = 1 + \left(\frac{E_{\rm imp}}{n_k E_{\rm roll}}\right)^{0.65}. \quad (46)$$

Our results show that catastrophic disruption producing fragments of various mass occurs when the impact energy becomes greater than $\sim 10 n_k E_{\rm break}$ as in the previous 2D simulations (Dominik & Tielens 1997; Wada et al. 2007). There is a tendency that the degree of disruption for aggregates composed of a large number of particles depends on their initial structures such as anisotropy of the collision cross section. However, this tendency is weaker in the 3D simulations than in the 2D.

We obtained an equation of state (EOS) of aggregates compressed by head-on collisions. If the EOS is written in terms of the density and the pressure of aggregates in the ordinary sense, it depends on the number of particles constituting the aggregates. In contrast, in terms of the fractal density ρ_f and the fractal pressure P_f the EOS is independent of the number of particles and is expressed by

$$P_f = \frac{d_f}{d_c - d_f} \frac{bE_{\rm roll}\rho_{f,1}}{m_1} \left(\frac{\rho_f}{\rho_{f,1}}\right)^{d_c/(d_c - d_f)}. \quad (47)$$

This EOS can be applied to a wide range of impact energies that induce outcomes from no restructuring up to the maximum compression. Therefore, the EOS obtained in the present study is applicable to reveal a wide range of the structural evolution of dust aggregates in protoplanetary disks.

The resultant aggregates created in our simulation still remain fluffy even though they are formed by head-on collisions. In realistic collisions, there are several factors to be taken into account for the future. For instance, offset collisions tend to produce elongated aggregates as shown by Wada et al. (2007). Rotation of

aggregates before a collision produces aggregates with a low fractal dimension (Paszun & Dominik 2006). These factors will make aggregates more fluffy than those formed in head-on collisions. Therefore, we conclude that dust aggregates (and planetesimals) growing through their mutual collisions would have very fluffy structures. A further study including these factors, such as offset collisions, will be required to confirm our conclusion.

We thank an anonymous reviewer for useful comments. We are grateful to T. Chigai for technical support on computer setup. This study was supported by the Grant-in-Aid for Scientific Research on Priority Areas "Development of Extrasolar Planetary Science" (16077203) and "Astrophysical Observations of New Phases of the Interstellar Gas at Submillimeter and THz Regions" (18026001), MEXT, Japan, and by the Grant-in-Aid from JSPS (18540227).

APPENDIX

EXPRESSION OF THE PRESSURE IN THE ORDINARY DIMENSION

In § 4 we defined the fractal volume V_f and the fractal density ρ_f of aggregates and derived the fractal pressure and the EOS of aggregates, using the fractal dimension d_c of maximum compressed aggregates. It is worthwhile to give an expression of the pressure in the ordinary sense here (i.e., having its dimension of N m^{-2}). This expression is readily obtained using the scaling law of r_g.

In the same way as in the discussion in § 4, a characteristic radius r_c (Mukai et al. 1992) of an aggregate having a gyration radius r_g is given by

$$r_c = \sqrt{\frac{5}{3}} r_g, \tag{A1}$$

where the factor $(5/3)^{1/2}$ is obtained by setting $d_c = 3$ in equation (21). The volume V of the aggregate is defined by

$$V \equiv \frac{4}{3}\pi r_c^3 = V_1 \left(\frac{r_g}{r_1}\right)^3, \tag{A2}$$

where $V_1 = (4\pi/3)[(5/3)^{1/2} r_1]^3$. Then, the specific volume v is given by

$$v \equiv \frac{V}{N} = V_1 \left(\frac{r_g}{r_1 N^{1/d_c}}\right)^3 N^{-(1-3/d_c)}. \tag{A3}$$

By the scaling law (eq. [13]), $r_g/(r_1 N^{1/d_c})$ is independent of N; thus, v is no longer an intensive variable. The density ρ of the aggregate is given by

$$\rho = \frac{m_1}{v} = \rho_1 \left(\frac{r_g}{r_1 N^{1/d_c}}\right)^{-3} N^{1-3/d_c}, \tag{A4}$$

where $\rho_1 = m_1/V_1$. The density ρ is not an intensive variable, either. Since $r_g/(r_1 N^{1/d_c}) \sim 1$ at the maximum compression, the maximum density $\rho_{\max}$ becomes

$$\rho_{\max} = \rho_1 N^{1-3/d_c}. \tag{A5}$$

Using the definition of the fractal density ρ_f (eq. [25]), ρ is expressed as a function of ρ_f,

$$\frac{\rho}{\rho_1} = \left(\frac{\rho_f}{\rho_{f,1}}\right)^{3/d_c} N^{1-3/d_c}. \tag{A6}$$

It is readily seen that ρ/ρ_1 equals $\rho_f/\rho_{f,1}$ if $d_c = 3$.

We define the pressure (or the strength) P of an aggregate by

$$d\epsilon_{\rm imp} = -P\, dv. \tag{A7}$$

Furthermore, using equations (13), (A3), and (A4), P is given by

$$P = -\frac{d\epsilon_{\rm imp}}{dv} = \frac{1}{3\alpha}\frac{bE_{\rm roll}\rho_1}{m_1}\left(\frac{\rho}{\rho_1}\right)^{(3\alpha+1)/(3\alpha)} N^{(3-d_c)/(3\alpha d_c)}, \tag{A8}$$

where $\alpha = 1/d_f - 1/d_c$. For $d_f = 2$ and $d_c = 2.5$, one has

$$P = \frac{10}{3}\frac{bE_{\rm roll}\rho_1}{m_1}\left(\frac{\rho}{\rho_1}\right)^{13/3} N^{2/3}. \tag{A9}$$

This indicates that the pressure depends on the number of particles N composing the aggregate as well as the density and increases with increasing N for a fixed density. Given the material density of a constituent particle, $\rho_m = 3m_1/(4\pi r_1^3)$, then $\rho_1 = (3/5)^{3/2}\rho_m$ and P is written by

$$P = \frac{10}{3}\left(\frac{3}{5}\right)^{-5}\frac{bE_{\rm roll}\rho_m}{m_1}\left(\frac{\rho}{\rho_m}\right)^{13/3}N^{2/3} \tag{A10}$$

for

$$\left(\frac{3}{5}\right)^{3/2}N^{-1/2} \lesssim \frac{\rho}{\rho_m} \lesssim \left(\frac{3}{5}\right)^{3/2}N^{-1/5}, \tag{A11}$$

where the upper and lower limits of the density are given by equation (A5) and the density of BCCA structure, respectively.

REFERENCES

Adachi, I., Hayashi, C., & Nakazawa, K. 1976, Prog. Theor. Phys., 56, 1756
Blum, J. 2004, in ASP Conf. Ser. 309, Astrophysics of Dust, ed. A. N. Witt, G. C. Clayton, & B. T. Draine (San Francisco: ASP), 369
———. 2006, Adv. Phys., 55, 881
Blum, J., Schräpler, R., Davidsson, B. J. R., & Trigo-Rodríguez, J. M. 2006, ApJ, 652, 1768
Blum, J., & Wurm, G. 2000, Icarus, 143, 138
Chokshi, A., Tielens, A. G. G. M., & Hollenbach, D. 1993, ApJ, 407, 806
Dominik, C., & Tielens, A. G. G. M. 1995, Philos. Mag. A, 72, 783
———. 1996, Philos. Mag. A, 73, 1279
———. 1997, ApJ, 480, 647
Goldreich, P., & Ward, W. R. 1973, ApJ, 183, 1051
Greenberg, J. M., Mizutani, H., & Yamamoto, T. 1995, A&A, 295, L35
Heim, L.-O., Blum, J., Preuss, M., & Butt, H.-J. 1999, Phys. Rev. Lett., 83, 3328
Israelachvili, J. 1992, Intermolecular and Surface Forces (2nd ed.; London: Academic)
Johnson, K. L. 1987, Contact Mechanics (Cambridge: Cambridge Univ. Press)
Johnson, K. L., Kendall, K., & Roberts, A. D. 1971, Proc. R. Soc. London A, 324, 301
Kempf, S., Pfalzner, S., & Henning, T. K. 1999, Icarus, 141, 388
Krause, M., & Blum, J. 2004, Phys. Rev. Lett., 93, 021103
Meakin, P. 1991, Rev. Geophys., 29, 317
Mukai, T., Ishimoto, H., Kozasa, T., Blum, J., & Greenberg, J. M. 1992, A&A, 262, 315
Nakagawa, Y., Nakazawa, K., & Hayashi, C. 1981, Icarus, 45, 517
Ormel, C. W., Spaans, M., & Tielens, A. G. G. M. 2007, A&A, 461, 215
Ossenkopf, V. 1993, A&A, 280, 617
Paszun, D., & Dominik, C. 2006, Icarus, 182, 274
Poppe, T., Blum, J., & Henning, T. 2000, ApJ, 533, 472
Schäfer, C., Speith, R., & Kley, W. 2007, A&A, 470, 733
Sirono, S. 2004, Icarus, 167, 431
Sirono, S., & Greenberg, J. M. 2000, Icarus, 145, 230
Smirnov, B. M. 1990, Phys. Rep., 188, 1
Suyama, T., Wada, K., & Tanaka, H. 2008, ApJ, submitted
Tanaka, H., Himeno, Y., & Ida, S. 2005, ApJ, 625, 414
Wada, K., Tanaka, H., Suyama, T., Kimura, H., & Yamamoto, T. 2007, ApJ, 661, 320
Weidenschilling, S. J. 1980, Icarus, 44, 172
———. 1984, Icarus, 60, 553
Weidenschilling, S. J., & Cuzzi, J. N. 1993, in Protostars and Planets III, ed. E. H. Levy & J. I. Lunine (Tucson: Univ. Arizona Press), 1031
Weidenschilling, S. J., & Ruzmaikina, T. V. 1994, ApJ, 430, 713
Wurm, G., Paraskov, G., & Krauss, O. 2005, Icarus, 178, 253